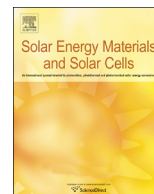




ELSEVIER

Contents lists available at ScienceDirect

Solar Energy Materials & Solar Cells

journal homepage: www.elsevier.com/locate/solmat

Generation of hot carrier population in colloidal silicon quantum dots for high-efficiency photovoltaics



Pengfei Zhang^{a,*}, Yu Feng^a, Xiaoming Wen^a, Wenkai Cao^a, Rebecca Anthony^{b,1}, Uwe Kortshagen^b, Gavin Conibeer^a, Shujuan Huang^{a,*}

^a School of Photovoltaic and Renewable Energy Engineering, the University of New South Wales, Sydney 2052, NSW, Australia

^b Mechanical Engineering Department, University of Minnesota, 111 Church Street SE, Minneapolis, MN 55455, USA

ARTICLE INFO

Article history:

Received 25 May 2015

Received in revised form

2 October 2015

Accepted 1 November 2015

Available online 17 November 2015

Keywords:

Hot carrier solar cell

Silicon quantum dots

Photoluminescence

State filling

ABSTRACT

Hot carrier generation in silicon (Si) quantum dots (QDs) is studied with power dependent continuous wave photoluminescence (CWPL) spectroscopy. By taking sub-band gap absorption into account, a modified Maxwell-Boltzmann-form equation was employed to achieve accurate theoretical fitting to the CWPL spectra of the Si QDs. As a fitting parameter, the excited carrier temperature was calculated. A steady-state carrier population was revealed with a temperature 500 K above room temperature under illumination equivalent to one standard sun (100 mW/cm²). In addition, since the carrier temperature increased with the power of illumination, a state filling effect is proposed as a reasonable cause for the elevated carrier temperature by comparative study of the CWPL spectra of Si QDs with three different sizes. These Si QDs show great potential for one of the steps towards a practical hot carrier solar cell (HCSC) device as high carrier temperatures can be achieved by state filling under mild illumination.

© 2015 Elsevier B.V. All rights reserved.

1. Introduction

Because of its natural abundance and non-toxicity, Si has long been chosen as the cornerstone of the microelectronics industry on which our modern information-based economy is built [1]. Furthermore, as its 1.12 eV bandgap matches the solar spectrum well, Si is suitable for photon capturing in a single-junction device, which gains its dominant position in photovoltaics (PV). Until recently, stimulated by the rapidly maturing solar cell industry of crystalline bulk Si, researchers have been keen to develop low-cost solution-processing techniques for colloidal semiconductor nanostructured solar cell devices [2–12], and more advanced third-generation solar cell concepts [13–16]. The former focuses on chemical synthesis of useful colloidal QDs and development of low-cost fabrication processes for thin film cells while the latter puts more emphasis in exploitation of new mechanisms that can be employed in advanced solar cell devices with efficiency beyond the Shockley-Queisser limit [17]. For the low-cost colloidal QDs

solar cells, a series of useful nanomaterials, such as PbS, PbSe and CdTe, have been successfully employed in fabrications of practical devices, achieving a certified efficiency as high as 8.55% [12]. On the other hand, several theoretical prototypes such as up conversion, multiple exciton generation (MEG) and hot carrier cells are comprehensively studied. With the development of colloidal QDs, these two important realms of PV research start to connect with each other recently. A wide range of colloidal QDs, especially PbS and PbSe, have also found their potentials in up conversion [18–20], tandem junctions [18,21–23] and multiple exciton generation (MEG) [24–29]. However, research on hot carrier solar cells (HCSCs) has been mainly carried out with thin solid film samples, e.g. III–V heterostructures [16,30–36]. Hence in this report we aim to apply solution processable Si QDs to HCSC, one kind of the advanced photovoltaic device that can achieve the highest theoretical efficiency [14].

Dissipation of heat from photo-generated carriers at high elevated levels to the surrounding lattice is one of the main mechanisms reducing solar cell efficiency. More than 30% of the incident solar power is thermalized through the lattice vibrations in this way even for the most efficient single-junction solar cells [31]. As one of the effective methods to overcome this problem, the concept of HCSC has been established [14]. In such a device, slowed carrier cooling could be realized in a hot carrier absorber in which the carrier–phonon interaction is remarkably restricted.

* Corresponding author. Tel.: +61404176111; fax: +61 2 9385 5456.

** Corresponding author. Tel.: +61 2 93855057; fax: +61 2 9385 5456.

E-mail addresses: larrymd.zhang@gmail.com (P. Zhang), sj.huang@unsw.edu.au (S. Huang).

¹ Present Address: Michigan State University, Engineering Building 428S, Shaw Lane East Lansing, MI 48824-1226, USA.

Thus a population of carriers at elevated energies is held for a time scale long enough to be extracted through energy selective contacts (ESCs). The main thermalization path for hot carriers is that they lose their energy by emitting optical phonons (lattice vibrations) on a timescale of a few picoseconds. One such optical phonon quickly decay into two acoustic phonons at half the energy and with equal but opposite momenta, via the Klemens anharmonicity mechanism [37]. Subsequently most of the energy is dissipated as heat in this way [35]. Theoretically, slowed carrier cooling can be achieved by a so called phonon bottleneck, which can block the optical phonon decay [35,38]. However, direct observation of phonon and hot carrier behavior is very challenging with existing techniques. Therefore, optical measurements have been systematically performed as a substitute and the phonon/hot carrier behavior are subsequently estimated from the photon-related spectra. In some cases, transient optical measurements, such as time resolved photoluminescence (TRPL) [39–44] and transient absorption [26,29,45,46] were carried out to analyze the hot-carrier related processes, whose lifetimes are generally on a picosecond timescale. Furthermore, the temperatures of the excitons have been recently calculated from the excitation power dependent CWPL spectra by Le Bris et al. [30] and Hirst et al. [31] in their respective research on solid state III–V heterostructures of quantum wells (QWs). Considering that solar cells usually operate in continuous illumination, the CWPL should have better applicability in investigating hot carrier dynamics. By assuming a Boltzmann–Maxwell distribution of carriers, they fitted the high-energy tail of their CWPL spectra with an exponential decay to retrieve a temperature at certain excitation power. They have shown an elevated carrier temperature with excitation power in the range of kW/cm² [30,31]. However it is not appropriate to transplant this method from QWs to QDs, as the later usually has a wider PL peak due to stronger quantum confinement and larger size distribution, in which case a suitable high energy tail is difficult to identify. In this work, a fitting strategy for Si QDs is developed based on the band-to-band recombination with size distribution incorporated. Successful fitting to the whole spectra of Si QDs of different sizes was achieved by using this new method, and a carrier population with a temperature ~500 K above room temperature was detected with a mild laser illumination ~100 mW/cm². Furthermore the evolution of carrier temperature with excitation power indicates that this elevated temperature possibly results from a state filling effect.

2. Materials and methods

2.1. Si colloidal QDs

The colloidal Si QDs studied here were synthesized by a gas-phase non-thermal plasma-assisted approach developed by Kortshagen et al. [47–49]. 1-dodecene was attached to the surface later in the liquid phase. Hence the Si QDs are easily dissolved into nonpolar solvent, in our case, chloroform. In addition, it is worth mentioning there are two important reasons for choosing this kind of colloidal Si QDs rather than those embedded in solid matrix. First, the colloidal Si QDs is solution processable, which could be easily employed to realize low-cost PV devices. Second, the colloidal Si QDs synthesized in plasma gas are relatively uniform in size and shape. The narrow size distribution can minimize the differences in the absorption cross-section of silicon quantum dots of each sample during the power dependent CWPL measurements, which was reported by Timmerman et al. to be another cause for the blue-shift and asymmetrical broadening of the PL peak under higher incident laser intensities [50].

Si QDs with three different sizes were studied in this work. To investigate the influences of the sizes of QDs on PL spectra, both X-ray diffraction (XRD, Fig. S1) and transmission electron microscopy (TEM, Fig. S2) were employed to determine the diameters of the QDs (the calculation process is presented in SI 1–2). The QD sizes calculated through Scherrer broadening of the XRD peaks are 2.6 nm, 3.7 nm and 6.0 nm, respectively. These sizes are in good agreement with the statistical averages collected from the TEM images, which are 2.4 nm, 3.8 nm and 6.3 nm. Size distributions for the three different samples were also obtained by measuring a certain number (~200 for 3.8 nm and 6.3 nm QDs, 45 for 2.4 nm due to the limitation of TEM resolutions) of QDs shown in HRTEM images (Fig. S3(a)–(c)) of Si QDs. The histograms in Fig. S3(d)–(f) show the number counting of QD diameters. It was found that the size distribution of the QDs is in Gaussian form, which can be expressed as:

$$F(D) \propto \frac{1}{\sigma} \exp \left[-\frac{(D-\bar{D})^2}{2\sigma^2} \right] \quad (1)$$

where \bar{D} and σ are the mean QD diameter and the standard deviation respectively. The size distribution of QDs will be taken into consideration in the following analysis of CWPL spectra.

2.2. CWPL spectroscopy of Si QDs

The excitation power dependent CWPL measurements were then performed on Si QDs of each size (2.4 nm, 3.8 nm and 6.3 nm). 30 μ L of Si QDs chloroform solution with a concentration of ~0.05 mg/mL was first spread onto a quartz substrate dropwisely and then allowed to dry at room temperature for 5 minutes. As-prepared samples were kept in a nitrogen filled desiccator to prevent oxidation. Relative PL measurements were carried out within one day after the sample preparation to minimize the aging effect [51]. Power dependent CWPL spectra were acquired with a homemade setup, which used a 406 nm GaN continuous laser diode as excitation. The laser was coupled with an Oriel Cornerstone i260 imaging monochromator to achieve an output power of 50 mW, which gave an initial incident power density of 1600 mW/cm² on a sample. Neutral density filters were subsequently inserted to adjust the power density from 100% to less than 0.1%. Finally the PL signals were collected by a cooled (–30 °C) Andor iVac Si CCD detector. Each set of power dependent PL spectra were measured at the same spot to avoid variation due to uneven deposition of drop casting.

Fig. 1 shows the CWPL spectra obtained from Si QDs of three sizes with incident light density ranging from ~1.6 to ~1600 mW/cm². The line shape of the PL spectrum is clearly asymmetrical broadened on the high energy side. Furthermore such broadening for Si QDs of 6.3 nm and 3.8 nm is visibly strengthened with the incident power, while that for 2.4 nm remains unchanged. It has been reported that this broadening is caused by an increased temperature of the carrier population (T_c), which could be quantitatively investigated by fitting a Maxwell-Boltzmann distribution to the high energy tail of the PL spectrum with Eq. (2) [30,31]

$$I_{pl}(E) \propto \exp \left(-\frac{E}{kT_c} \right) \quad (2)$$

where I is the intensity of PL, k is the Boltzmann constant, E is energy of the emitted photons, which can be calculated by $E = h\nu = hc/\lambda$, h is the Planck constant, c is the speed of light, and λ is the photon wavelength.

Download English Version:

<https://daneshyari.com/en/article/77694>

Download Persian Version:

<https://daneshyari.com/article/77694>

[Daneshyari.com](https://daneshyari.com)